Structure, thermal, and transport properties of the clathrates $Sr_8Zn_8Ge_{38}$, $Sr_8Ga_{16}Ge_{30}$, and $Ba_8Ga_{16}Si_{30}$

Liyan Qiu and Ian P. Swainson
Steacie Institute for Molecular Sciences, National Research Council of Canada, Chalk River Laboratories, Chalk River, Ontario, Canada K0J 1J0

George S. Nolas
Department of Physics, University of South Florida, Tampa, Florida 33620-5700, USA

Mary Anne White
Department of Chemistry and Institute for Research in Materials, Dalhousie University, Halifax, Nova Scotia, Canada B3H 4J3
(Received 22 January 2004; published 27 July 2004)

The structural parameters, thermal properties, and transport properties of three type I clathrates, namely $Sr_8Zn_8Ge_{38}$, $Sr_8Ga_{16}Ge_{30}$, and $Ba_8Ga_{16}Si_{30}$, have been determined at or below room temperature. The structural parameters of these clathrates were determined by powder neutron diffraction. Their lattice thermal expansion is two to four times greater than that of the diamond phases of silicon and germanium, consistent with more anharmonic lattice vibrations. From the temperature dependence of the isotropic atomic displacement parameters, the estimated rattling frequencies of guests in the large cages of these clathrates are in the range 50–60 cm^{-1}. The heat capacities of these three clathrate materials increase smoothly with increasing temperatures and approach the Dulong–Petit value around room temperature. The Grüneisen parameter of these materials is constant between 100 and 300 K but increases below 100 K, due to the dominance of the low-frequency guest-rattling modes. The room-temperature electrical resistivity and the Seebeck coefficient show that these materials are metallic. The temperature profile of the thermal conductivities and calculated phonon mean free paths of these materials show glasslike behavior, although they are crystalline materials, indicating strong resonant scattering of heat-carrying acoustic phonons via the rattling of the guests in the clathrate cages.

DOI: 10.1103/PhysRevB.70.035208 PACS number(s): 82.75.−z, 65.40.−b, 61.12.−q

I. INTRODUCTION

Silicon, germanium, and tin clathrates can form inclusion compounds similar to those of type I and type II clathrate hydrates in which the host forms cages in which guests are included.[1] Generally, clathrate structures are not stable if the guests are removed. In type I clathrates, general formula M_xX_{46}, 46 framework atoms form the unit cell of a simple cubic structure, space group $Pm\bar{3}n$, where M and X represent the guest metal atoms and the framework atoms, respectively. Each unit cell contains two small 20-atom cages, pentagonal dodecahedra, X_{20}, and six large 24-atom cages, tetrakaidecahedra, X_{24},[2] as shown in Fig. 1. The transport properties of clathrates can be significantly changed by doping different guests in the cages of the framework.[3–10]

The thermal conductivities of these novel materials can be significantly lower than their diamond phases and glasslike, although clathrates have a well-defined crystalline structure.[3,7,9–11] The temperature profile of the thermal conductivity of clathrates not only depends on the guests, but also on the framework atoms.[4,5,7,9] As first deduced for clathrate hydrates,[12] the glasslike thermal conductivity of clathrates is due to the strong scattering of heat-carrying acoustic phonons by the rattling of the guests in the cages.[3,7,9] The glasslike thermal conductivity, high electrical conductivity, high Seebeck coefficient, and their high stability (in air, strong acids, and bases) make clathrates promising thermoelectric materials for solid-state cooling devices and power generation.[7,13,14]

Thermal and transport properties are important to clathrates since they determine the thermoelectric efficiency and hence the utility of these materials. For example, thermal

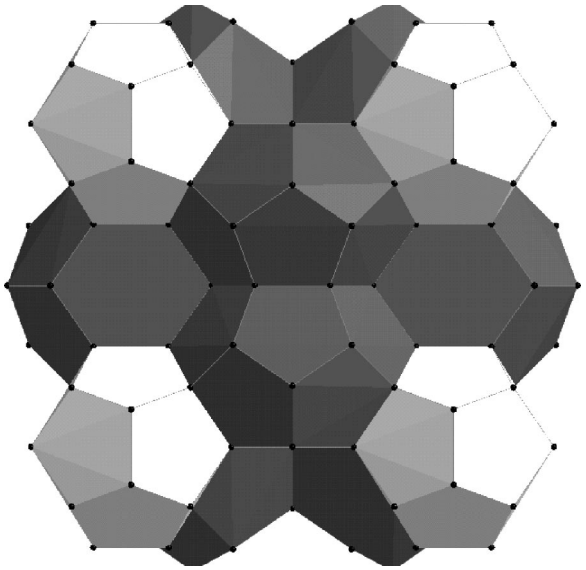

FIG. 1. Structure of type I clathrates where the X_{20} cage is white and the X_{24} cage is black.

TABLE I. Powder neutron-diffraction data results for $Sr_8Zn_8Ge_{38}$, $Sr_8Ga_{16}Ge_{30}$, and $Ba_8Ga_{16}Si_{30}$.

Chemical formula	$Sr_8Zn_8Ge_{38}$	$Sr_8Ga_{16}Ge_{30}$	$Ba_8Ga_{16}Si_{30}$
Space group	$Pm\bar{3}n$	$Pm\bar{3}n$	$Pm\bar{3}n$
$T(K)$	287.8	274.9	300.1
a(Å)	10.7044(4)	10.7380(3)	10.5532(4)
Density/g cm^{-3}	5.391	5.357	4.319
Data points	1557	1598	1562
R_{wp}	0.0677	0.0619	0.0468
R_p	0.0537	0.0485	0.0362

conductivity is an important quantity in the dimensionless figure of merit, ZT. The measurement of heat capacity provides information concerning thermodynamic stability of materials and lattice vibration anharmonicity. The structure and thermal expansion of these materials can be determined directly from powder neutron or x-ray diffraction, and the dynamical properties of both guests and framework atoms can be inferred by examining the variation of atomic displacement parameters (ADP's) with temperature.[6,11,15]

In this paper, the structural parameters and heat capacities of three type I clathrates, $Ba_8Ga_{16}Si_{30}$, $Sr_8Ga_{16}Ge_{30}$, and $Sr_8Zn_8Ge_{38}$, at and below room temperature are presented. The thermal conductivity, electrical resistivity and Seebeck coefficient of the newly synthesized clathrate $Sr_8Zn_8Ge_{38}$ are also presented. The Grüneisen parameters of all these clathrate materials were evaluated in order to quantify anharmonicity of lattice vibrations.

II. EXPERIMENTAL METHODS

A. Materials synthesis

The three type I clathrate materials were synthesized by mixing stoichiometric quantities of the high-purity elements and reacting for three days at 950 °C inside a pyrolytic boron nitride crucible that was itself sealed inside a fused quartz ampoule. The ampoule was evacuated and back-filled with high-purity argon gas. In the case of the Ge-clathrates, the resulting boules consisted of small single-crystal grains while the Si-clathrate specimen was a loosely sintered powder. All specimens were stable in air or water.

B. Powder neutron powder diffraction

Powder neutron-diffraction data were collected between 15 K and 300 K at the C2 diffractometer at Chalk River Laboratories, Canada, which consists of an 800-wire BF_3 detector, each wire 0.1° apart. Powder samples are sealed in a vanadium can, 0.5 cm diam, and a closed-cycle refrigerator was used to cool the samples. The temperature was monitored using calibrated Si diodes. A neutron wavelength of 1.32993(5) Å was used, calibrated with an external Si standard. The data were taken in two banks between 5° and 80° and between 37° and 117° in 2θ. The number of data points in each refinement is slightly different (Table I) because some low angle points below the first Bragg peaks were chopped during data refinement.

C. Heat-capacity measurements

Heat capacity was measured from ~30 to 310 K. The measurement of heat capacity was carried out by an adiabatic calorimeter which was operated in a heat-pulse mode.[16] The calorimeter has been tested previously with Calorimetry Conference standard benzoic acid, giving results that agreed with the literature to within 0.5%. The sample was loaded in a glove box filled with dry nitrogen. The calorimeter was sealed in a helium atmosphere in order to increase the heat exchange rate and decrease the relaxation time to reach thermal equilibrium.

D. Measurement of transport properties

Four-probe electrical resistivity, steady-state Seebeck coefficient, and thermal conductivity measurements were performed in a radiation-shielded vacuum probe inside a closed-cycle refrigerator. Heat losses via conduction through lead wires and radiation were determined in separate experiments and the thermal conductivity data corrected accordingly. These corrections were approximately 5% of the total near room temperature and less at lower temperatures.

III. RESULTS AND DISCUSSION

A. Structures

The Rietveld method GSAS software was used to refine the structure. The profile was modeled using the standard Cagliotti model and the background was defined by a fourth-order polynomial. Neutron absorption was calibrated but it had only a minor effect on the structural refinement. The 24j split-site model for X_{24} guest was used in the structural refinement and the initial atomic positions for data fitting were taken from the literature.[17]

Three different isotropic ADP's, U_{iso}, corresponding to guests in small cages (X_{20}), large cages (X_{24}), and the framework atoms were set as adjustable parameters. We did not distinguish ADP's of framework atoms at different sites.

In the neutron powder pattern, $Ba_8Ga_{16}Si_{30}$ showed a small amount of silicon (2%). $Sr_8Ga_{16}Ge_{30}$ did not show any other phases while $Sr_8Zn_8Ge_{38}$ showed a small amount of Ge and $SrZn_2Ge_2$, totalling 2%. These impurities were included in the Rietveld refinement and are expected to have no significant effect on the determination of the lattice parameters.

All three samples have a simple primitive cubic structure with space group $Pm\bar{3}n$. The lattice parameters and the atomic positions of each material near room temperature are listed in Tables I and II, respectively. Full lattice parameters and atomic displacement parameters have been deposited.

In $Ba_8Ga_{16}Si_{30}$, there are four different bond lengths between frameworks atoms. They are 2.506(6) Å, 2.467(3) Å, 2.441(2) Å, and 2.366(7) Å at 300.1 K. The framework atoms are linked through tetrahedra. The bond angles between framework atoms range from 105.81(12)° to 124.17(7)°.

TABLE II. Fraction fixed structural refinement of three clathrates.

	T (K)	x	y	z	Fraction	$U_{iso}(10^{-2}Å^2)$	Mult
$Sr_8Zn_8Ge_{38}$	287.8						
Sr(1)		0.0000	0.0000	0.0000	1.0000	2.9(3)	2
Sr(2)		0.2500	0.5196(15)	0.0196(15)	0.2500	4.2(6)	24
Zn(3)		0.0000	0.3102(2)	0.1167(2)	0.1739	0.91(6)	24
Ge(4)		0.0000	0.3102(2)	0.1167(2)	0.8261	0.91(6)	24
Zn(5)		0.1841(2)	0.1841(2)	0.1841(2)	0.1739	0.91(6)	16
Ge(6)		0.1841(2)	0.1841(2)	0.1841(2)	0.8261	0.91(6)	16
Zn(7)		0.2500	0.0000	0.5000	0.1739	0.91(6)	6
Ge(8)		0.2500	0.0000	0.5000	0.8261	0.91(6)	6
$Sr_8Ga_{16}Ge_{30}$	274.9						
Sr(1)		0.0000	0.0000	0.0000	1.0000	1.6(3)	2
Sr(2)		0.2500	0.5230(9)	0.0203(9)	0.2500	4.3(6)	24
Ga(3)		0.0000	0.3092(2)	0.1170(2)	0.3478	0.74(6)	24
Ge(4)		0.0000	0.3092(2)	0.1170(2)	0.6522	0.74(6)	24
Ga(5)		0.1843(1)	0.1843(1)	0.1843(1)	0.3478	0.74(6)	16
Ge(6)		0.1843(1)	0.1843(1)	0.1843(1)	0.6522	0.74(6)	16
Ga(7)		0.2500	0.0000	0.5000	0.3478	0.74(6)	6
Ge(8)		0.2500	0.0000	0.5000	0.6522	0.74(6)	6
$Ba_8Ga_{16}Si_{30}$	300.1						
Ba(1)		0.0000	0.0000	0.0000	1.0000	0.8(0.2)	2
Ba(2)		0.2500	0.5083(22)	0.0084(22)	0.2500	2.6(0.4)	24
Ga(3)		0.0000	0.3065(2)	0.1196(2)	0.3478	0.93(6)	24
Si(4)		0.0000	0.3065(2)	0.1196(2)	0.6522	0.93(6)	24
Ga(5)		0.1855(2)	0.1855(2)	0.1855(2)	0.3478	0.93(6)	16
Si(6)		0.1855(2)	0.1855(2)	0.1855(2)	0.6522	0.93(6)	16
Ga(7)		0.2500	0.0000	0.5000	0.3478	0.93(6)	6
Si(8)		0.2500	0.0000	0.5000	0.6522	0.93(6)	6

In $Sr_8Ga_{16}Ge_{30}$, four different bond lengths between framework atoms are found: 2.514(4) Å, 2.4972(15) Å, 2.4969(20) Å, and 2.446(5) Å. The framework bond length in $Sr_8Ga_{16}Ge_{30}$ is longer than those in $Ba_8Ga_{16}Si_{30}$ due to the larger atomic radius of Ge compared with Si. The bond angles range from 104.80(9)° to 124.87(4)°.

In $Sr_8Zn_8Ge_{38}$, the four different bond lengths between framework atoms are 2.503(6) Å, 2.497(22) Å, 2.477(3) Å, and 2.444(7) Å. Most of them are slightly shorter than those in $Sr_8Ga_{16}Ge_{30}$ but longer than that of $Ba_8Ga_{16}Si_{30}$. The bond angle between the framework atoms of $Sr_8Zn_8Ge_{38}$ varies from 104.20(4)° to 125.11(7)°, similar to those in $Sr_8Ga_{16}Ge_{30}$.

In the data fitting for $Sr_8Zn_8Ge_{38}$, the site preference of framework atoms was tested by turning the fraction flags "on," as the contrast between Zn and Ge is good. It was

TABLE III. Site preference structural refinement for $Sr_8Zn_8Ge_{38}$ at 287.8 K.

	x	y	z	Fraction	$U_{iso}(10^{-2}Å^2)$	Mult
Sr(1)	0.0000	0.0000	0.0000	1.0000	1.8(3)	2
Sr(2)	0.2500	0.5196(13)	0.0194(13)	0.2500	4.2(6)	24
Zn(3)	0.0000	0.3104(2)	0.1167(2)	−0.02(8)	1.06(5)	24
Ge(4)	0.0000	0.3104(2)	0.1167(2)	1.02(8)	1.06(5)	24
Zn(5)	0.1837(2)	0.1837(2)	0.1837(2)	0.10(8)	1.06(5)	16
Ge(6)	0.1837(2)	0.1837(2)	0.1837(2)	0.90(8)	1.06(5)	16
Zn(7)	0.2500	0.0000	0.5000	0.88(7)	1.06(5)	6
Ge(8)	0.2500	0.0000	0.5000	0.12(7)	1.06(5)	6

TABLE IV. Calculated coordination information for the X_{20} and X_{24} sites. M is the guest and X is the framework atom at the corner of the cages.

X_{20}	M-X (Å)	M-X (Å)		Unit cell volume (Å^3)	Volume X_{20} (Å^3)
$Sr_8Zn_8Ge_{38}$	3.4133(8)	3.5477(12)		1226.55	121.61
$Sr_8Ga_{16}Ge_{30}$	3.4277(8)	3.5499(12)		1238.14	122.14
$Ba_8Ga_{16}Si_{30}$	3.3907(8)	3.4721(12)		1175.31	115.25
X_{24}	M-X (Å)	M-X (Å)	M-X (Å)	M-X (Å)	Volume X_{20} (Å^3)
$Sr_8Zn_8Ge_{38}$	3.5847(8)	3.7846(4)	3.9769(8)	4.1533(4)	163.89
$Sr_8Ga_{16}Ge_{30}$	3.6031(8)	3.7964(4)	3.9883(8)	4.1615(4)	165.65
$Ba_8Ga_{16}Si_{30}$	3.5670(8)	3.7311(4)	3.9130(8)	4.0585(4)	157.47

found that Zn strongly prefers the 6*c* site and has occupation fractions 0.88 ± 0.07 at 6*c*, 0.10 ± 0.08 at 16*i*, and -0.02 ± 0.08 at 24*k*, shown in Table III. Therefore, almost all Zn atoms occupy the 6*c* sites. The calculated total number of Zn atoms per formula unit based on occupation fraction at each site is 7 ± 3. This result is reasonable considering that we did not constrain the total number of framework atoms during the data refinement. The variation of these values with temperature is within the errors of calculation. $Sr_8Ga_{16}Ge_{30}$ and $Ba_8Ga_{16}Si_{30}$ also show a higher occupation fraction for Ga atoms at site 6*c* than other sites but a weaker preference than for Zn in $Sr_8Zn_8Ge_{38}$, although this may also reflect the weaker contrast between Ge and Ga. The results agree with a previous experimental report[13,18] and theoretical calculation that the 6*c* position has a lower site energy than the 24*k* and 16*i* sites.[19] The site preference can result in distortion of the clathrate framework[19] as we observed in our structural refinement.

It is important to know the cage size in order to predict synthesis of new clathrates and to understand the host-guest interactions. If the size of guests is larger than the free space of the cage, the guest cannot be included in the cages. Hence, the polyhedral volumes of X_{20} and X_{24} of the three clathrate materials were calculated using the programs VOLCAL[20] and IVTON,[21] and the results are listed in Table IV. VOLCAL and IVTON gave identical values for the more regular X_{20}, but neither proved capable of calculating the volume of the X_{24} site accurately (VOLCAL crashed while IVTON gave answers close to but not exactly those presented in Table IV and showed significant variations for very small changes in the position of the M atom from the centroid). There are two X_{20} sites and six X_{24} sites, which completely tile the volume of the unit cell, so the volume of X_{24} was calculated via the difference. We found that the cages of $Sr_8Zn_8Ge_{38}$ are larger than for $Ba_8Ga_{16}Si_{30}$ but smaller than for $Sr_8Ga_{16}Ge_{30}$.

The isotropic ADP's, U_{iso}, determined from powder neutron diffraction, are shown in Figs. 2–4. We noticed that the U_{iso} values of the guests and framework atoms are slightly changed when the fraction flags are turned on. However, no significant effect is observed on the atomic positions (see Tables II and III for $Sr_8Zn_8Ge_{38}$) nor the slope of U_{iso} versus temperatures. The ADP's of framework atoms in these materials are smaller than those of their guests and increase slowly with temperature.

The ADP's of guests in X_{24} are much larger than those of guests in X_{20}. Even at the lowest experimental temperature, the U_{iso} values of guests in X_{24} still are relatively large. The large ADP probably indicates that Sr(2) and Ba(2) in X_{24} undergo both dynamical and static disorder.[5,11,22]

Among the Ge clathrates, the ADP of Sr(2) in $Sr_8Ga_{16}Ge_{30}$ is greater than in $Sr_8Zn_8Ge_{38}$. For $Ba_8Ga_{16}Si_{30}$, Ba(2) has the smallest ADP of all the X_{24} cages due to the relatively small size of the cage and large mass of the guest. The larger ADP of the framework atoms in $Ba_8Ga_{16}Si_{30}$ could be due to the smaller mass of the Si framework atom.

The isotropic ADP has been successfully used to evaluate the Debye temperature, θ_D, of framework atoms,[4–6,11,22] using $U_{iso}=3h^2/(mk_B\theta_D^2 4\pi^2)T$, where h is Planck's constant, k_B is the Boltzmann constant, and m is the mean atomic mass of the framework. The estimated Debye temperatures, θ_D^{ADP}, extracted from the slope of U_{iso}-T straight lines and listed in Table V, are comparable with those determined from heat-

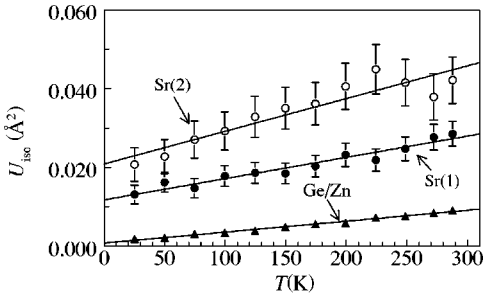

FIG. 2. Isotropic atomic displacement parameter in $Sr_8Zn_8Ge_{38}$.

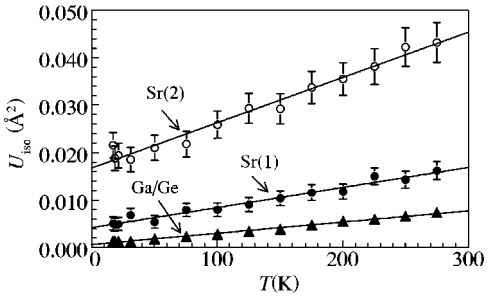

FIG. 3. Isotropic atomic displacement parameter in $Sr_8Ga_{16}Ge_{30}$.

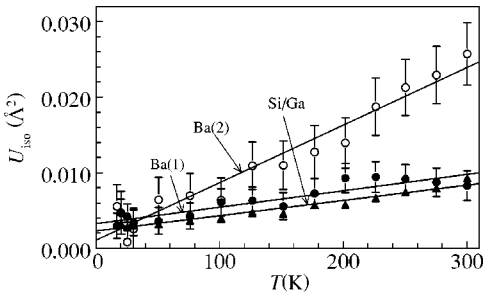

FIG. 4. Isotropic atomic displacement parameter in $Ba_8Ga_{16}Si_{30}$.

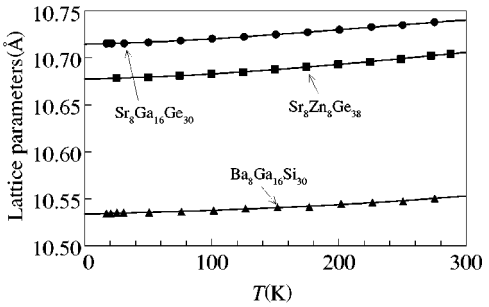

FIG. 5. Lattice parameters of $Sr_8Ga_{16}Ge_{30}$ and $Sr_8Zn_8Ge_{38}$ and $Ba_8Ga_{16}Si_{30}$ as functions of temperature.

capacity data, also listed in the same table (*vide infra*).

The rattling frequencies of guests also can be estimated from the slope of their temperature-dependent ADP's with the equation,[5,6,22] $U_{iso}=k_BT/m(2\pi\nu)^2$; these frequencies are listed in Table V. The estimated rattling frequencies of Sr in $Sr_8Ga_{16}Ge_{30}$ agree well with those from powder x-ray diffraction,[13] earlier neutron diffraction,[11] estimates from experimental thermal conductivity,[5,7,9] and Raman scattering measurements.[23] The estimated rattling frequency of Sr in the large cage of $Sr_8Zn_8Ge_{38}$ agrees well with that estimated from the "resonant dip" of its thermal conductivity, as discussed below.

The lattice vibration contribution to the thermal conductivity at room temperature can be determined with the equation $k=C\nu\lambda/3$, where the mean free path of phonons λ can be taken as the distance between guests in X_{24} cages[22] as estimated from the current neutron powder diffraction refinements. Although accurate determination of the speed of sound, ν, requires elastic properties which are not available currently, it can be estimated from $\nu=(2\pi\theta_Dk_B/h)/(6\pi^2n)^{1/3}$, where n is the number of atoms per unit volume. These values of ν are listed in Table V. On this basis, the lattice thermal conductivities were calculated (results in Table V) and agree reasonably well with the experimental values presented below.

B. Thermal expansion

The lattice parameters of these cubic materials at different temperatures are shown in Fig. 5. Those of $Ba_8Ga_{16}Si_{30}$ and $Sr_8Ga_{16}Ge_{30}$ agree well with those reported around room temperature.[9] $Ba_8Ga_{16}Si_{30}$ has the smallest lattice parameter and $Sr_8Ga_{16}Ge_{30}$ has a lattice parameter slightly greater than that of $Sr_8Zn_8Ge_{38}$.

The unit cell of these materials shows smooth expansion with increasing temperature. At temperatures above 100 K, the lattice of these materials expands almost linearly. The lattice parameters within the whole experimental temperature region were fit to a third-order polynomial, $a=a_0+a_1T+a_2T^2+a_3T^3$, where the values of a_0, a_1, a_2, and a_3 are listed in Table VI. The volume thermal expansion coefficient, α, was calculated with the equation $\alpha=3/a(\partial a/\partial T)_P$. At 300 K, $Sr_8Ga_{16}Ge_{30}$, $Sr_8Zn_8Ge_{38}$, and $Ba_8Ga_{16}Si_{30}$ have volume thermal expansion coefficients of 2.7×10^{-5} K^{-1}, 3.6×10^{-5} K^{-1}, and 3.2×10^{-5} K^{-1}, respectively.

Compared with the diamond phases Si and Ge,[24,25] both Si clathrates and Ge clathrates show greater thermal expansion at the same temperature. For example, the room-temperature thermal expansion coefficients of $Sr_8Zn_8Ge_{38}$ are about twice that of the diamond phase of germanium[24] while that of $Ba_8Ga_{16}Si_{30}$ is more than four times greater than that of the diamond phase of silicon.[24,25] The greater thermal expansion values for the clathrates could be due to more anharmonic lattice vibrations and host-guest interactions. A similar phenomenon also has been observed in clathrate hydrates.[26]

C. Heat capacity

The experimental heat capacity, C_p, shown in Fig. 6 (data deposited) was found to increase smoothly with temperature in the experimental temperature range.

The isochoric heat capacity, C_v, is theoretically more useful than C_p and, for these cubic materials, can be calculated from the equation $C_p-C_v=\alpha^2TV/\kappa_T$, where κ_T is the isothermal compressibility. From the present lattice parameters and the experimental bulk modulus[27] for $Sr_8Ga_{16}Ge_{30}$, (C_p-C_v) is 10 J K^{-1} mol^{-1} at 300 K, corresponding to 0.7% of C_p at room temperature. The bulk modulus of $Sr_8Ga_{16}Ge_{30}$ (Ref. 27) also was used for the estimate of (C_p-C_v) of $Sr_8Zn_8Ge_{38}$ and Na_8Si_{46} (Ref. 28) for $Ba_8Ga_{16}Si_{30}$. The estimated value of (C_p-C_v) at 300 K is 0.8% of C_p for $Sr_8Zn_8Ge_{38}$ and 5% of C_p for $Ba_8Ga_{16}Si_{30}$, respectively. The value of $(C_p-C_v)/C_p$ decreases as temperature drops. Even accounting

TABLE V. Selected thermal and dynamic properties of three clathrates.

	$\theta_D^{C_P}$ (K)	θ_D^{ADP} (K)	ω_1 (cm^{-1})	ω_2 (cm^{-1})	ν (km s^{-1})	λ (Å)	k_{cal} (W m^{-1} K^{-1})
$Ba_8Ga_{16}Si_{30}$	430	420	110	59	3.9	5.5	1.4
$Sr_8Zn_8Ge_{38}$	290	270	70	56	2.6	5.7	0.95
$Sr_8Ga_{16}Ge_{30}$	320	290	80	53	2.8	5.8	0.99

TABLE VI. Parameters for the polynomial function, $a=a_0+a_1T+a_2T^2+a_3T^3$, used to fit lattice parameters.

	a_0 (Å)	a_1 (10^{-5} K^{-1})	a_2 (10^{-7} K^{-2})	a_3 (10^{-10} K^{-3})
$Ba_8Ga_{16}Si_{30}$	10.534	2.8962	0.7128	1.4583
$Sr_8Zn_8Ge_{38}$	10.677	1.2428	4.2851	−5.2059
$Sr_8Ga_{16}Ge_{30}$	10.715	2.2205	3.8149	−5.7337

for (C_p-C_v), the heat capacity (C_p or C_v) for all these clathrates at room temperature approaches the Dulong-Petit value, $162R$ (1347 J K^{-1} mol^{-1}), where R is the gas constant. This means that the optic modes of these clathrate materials have rather low frequencies and all optic modes and acoustic modes are nearly fully excited around room temperature.

The effective Debye temperature (i.e., treating all the lattice modes as Debye-like) calculated from the heat capacity of these three clathrates is a temperature-dependent quantity. The maximum effective Debye temperatures of these clathrates from heat capacities are listed in Table V as θ_D^{Cp}. The higher effective Debye temperature of $Ba_8Ga_{16}Si_{30}$ compared with the germanium clathrates can be attributed to the stiffer Si-Si bonds compared with Ge-Ge bonds, consistent with the results presented above from neutron diffraction. Compared with Na_8Si_{46},[15] the lower effective Debye temperature of $Ba_8Ga_{16}Si_{30}$ reveals that the replacement of Si atoms by Ga decreases the stiffness of the framework.

D. Grüneisen parameter

The Grüneisen parameter, γ, is a measurement of anharmonicity of lattice vibrations. For cubic phases, a convenient way to obtain the overall Grüneisen parameter is given by $\gamma=\alpha V/\kappa_T C_v$. The quantities required to calculate γ are available here, and the values of γ of these three clathrates as functions of temperature are shown in Fig. 7. The Grüneisen parameters of $Ba_8Ga_{16}Si_{30}$, $Sr_8Ga_{16}Ge_{30}$, and $Sr_8Zn_8Ge_{38}$ have similar temperature profiles and are almost constant from 100 to 300 K. The values for $Sr_8Ga_{16}Ge_{30}$ and $Sr_8Zn_8Ge_{38}$ are almost the same, but the smaller value of the Grüneisen parameter for $Ba_8Ga_{16}Si_{30}$ correlates with the stiffer framework of the silicon clathrate.

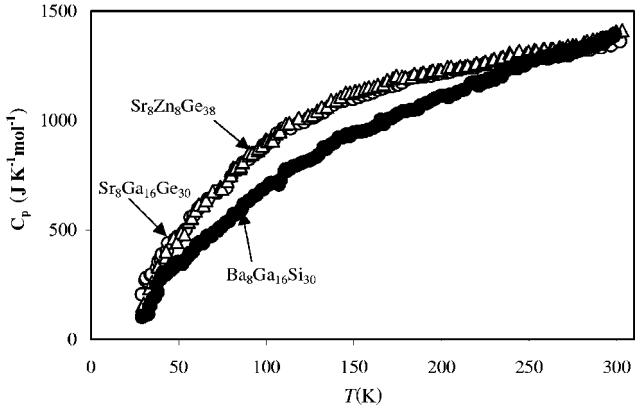

FIG. 6. Experimental heat capacity of $Sr_8Ga_{16}Ge_{30}$ (○), $Sr_8Zn_8Ge_{38}$ (Δ), and $Ba_8Ga_{16}Si_{30}$ (●).

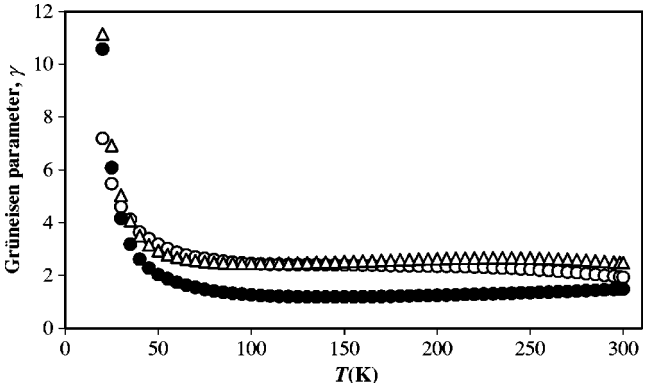

FIG. 7. Grüneisen parameters of $Ba_8Ga_{16}Si_{30}$ (●), $Sr_8Ga_{16}Ge_{30}$ (○), and $Sr_8Zn_8Ge_{38}$ (Δ).

According to thermodynamic principles, the lattice expansion and hence the Grüneisen parameter should reach zero as the temperature approaches absolute zero. However, the Grüneisen parameters of these three clathrates increase with decreasing temperature below 100 K. Similar behavior has been observed in Na_8Si_{46},[15] and clathrate hydrates[29] due to the existence of the low vibrational frequencies of the guests. These low-frequency modes can dominate the low-temperature Grüneisen parameter.[15]

E. Transport properties

The values of resistivity (ρ), Seebeck coefficient (S), and thermal conductivity (κ) of these three clathrates at 298 K are presented in Table VII. The temperature dependence of the Seebeck coefficient and the resistivity of $Sr_8Zn_8Ge_{38}$ are shown in Fig. 8. The temperature dependence of these properties for the other clathrates has been previously published.[7,9]

The resistivity of these three clathrates at room temperature is within the region of metals. Replacing Ga by Zn atoms in the framework results in a lower electrical resistivity for $Sr_8Zn_8Ge_{38}$ as compared with $Sr_8Ga_{16}Ge_{30}$, however this may be due to a less than optimum stoichiometry in the case of $Sr_8Zn_8Ge_{38}$. The negative S may be an indication that the majority of carriers are electrons.

The room-temperature values of lattice thermal conductivity of these three materials (Table VII) are low, comparable to that of vitreous silica ($\kappa\sim 1.2$ W m^{-1} K^{-1}).[30] The temperature dependence of thermal conductivity of $Sr_8Zn_8Ge_{38}$ and $Sr_8Ga_{16}Ge_{30}$ (Fig. 9) also shows a glasslike

TABLE VII. Electrical resistivity ρ, Seebeck coefficient S, lattice thermal conductive κ, and electronic thermal conductivity κ_e at $T=298$ K.

	ρ (mΩ cm)	S (μV K^{-1})	κ (W m^{-1} K^{-1})	κ_e (W m^{-1} K^{-1})
$Ba_8Ga_{16}Si_{30}$	2.0	−66	1.2	0.36
$Sr_8Zn_8Ge_{38}$	0.33	−24	1.9	2.2
$Sr_8Ga_{16}Ge_{30}$	2.0	−115	1.0	0.36

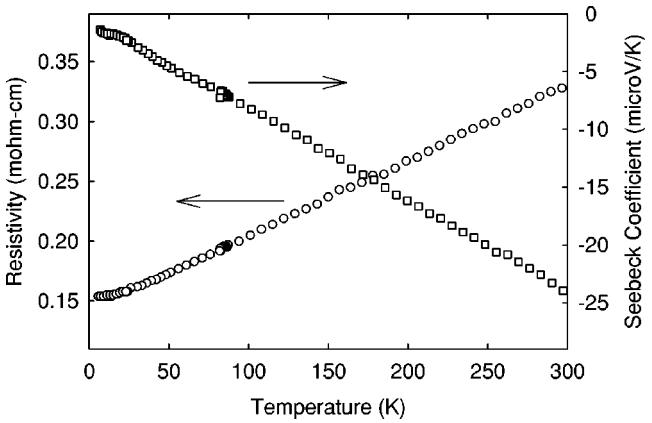

FIG. 8. Temperature dependence of the Seebeck coefficient and resistivity of $Sr_8Zn_8Ge_{38}$.

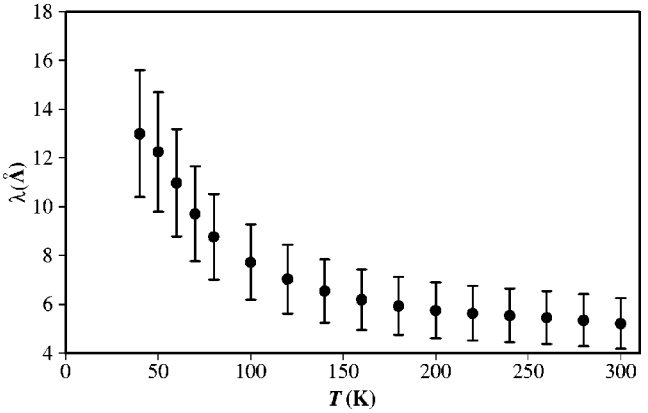

FIG. 10. Phonon mean free path of $Sr_8Ga_{16}Ge_{30}$.

behavior,[29] although these clathrates are typical crystalline materials.

The thermal conductivity of $Sr_8Zn_8Ge_{38}$ shows a temperature profile similar to that of $Sr_8Ga_{16}Ge_{30}$ over the whole experimental temperature (Fig. 9). Both $Sr_8Ga_{16}Ge_{30}$ and $Sr_8Zn_8Ge_{38}$ show a "resonance dip" around $T=20$ K. Such a dip is an indication of strong resonant scattering via the guest vibrations at an energy[7] $hc\omega$, where c is the speed of light and ω is in wave numbers. The estimated rattling frequency of Sr in $Sr_8Zn_8Ge_{36}$ and $Sr_8Ga_{16}Ge_{30}$ is 54 cm^{-1} using[31] $hc\omega=3.9kT$, which agrees very well with that estimated from the isotropic ADP's discussed above.

Ba is more massive than the Ga and Si framework atoms, and Ba is similar in size to the Si_{20} and Si_{24} cages. Therefore, there is a minimal dynamic disorder and thus not as strong a phonon-coupling mechanism as compared to Sr in $Sr_8Ga_{16}Se_{30}$. Hence one would predict $Ba_8Ga_{16}Si_{30}$ to show higher thermal conductivity than $Sr_8Ga_{16}Se_{30}$, as observed. This picture is confirmed by our neutron-scattering measurements, as discussed above.

The low thermal conductivity of these clathrates can also be understood from the phonon mean free path using the Debye model, $\kappa=Cv\lambda/3$. As an example, Fig. 10 shows the temperature-dependent mean free path of phonons of $Sr_8Ga_{16}Ge_{30}$ using experimental sound speed,[11] thermal conductivity, and heat capacity. At room temperature, the calculated mean free path of $Sr_8Ga_{16}Ge_{30}$ is very short, about 5 Å, due to the efficient scattering of heat-carrying phonons by the rattling of guests in the cages. Compared with Na_8Si_{46},[4] $Sr_8Ga_{16}Ge_{30}$ has a shorter phonon mean free path, indicating that Sr in $Sr_8Ga_{16}Ge_{30}$ is a more efficient scatterer of acoustic phonons than is Na in Na_8Si_{46}.

The electronic thermal conductivity, κ_e, of the three clathrates was estimated using the Wiedemann-Franz law, $\kappa_e=LT/\rho$, where $L=2.44\times10^{-8}$ W Ω K^{-2}. The κ_e values also are listed in Table VII. The low electronic thermal conductivity in $Sr_8Ga_{16}Ge_{30}$ and $Ba_8Ga_{16}Si_{30}$ indicates that the lattice component of thermal conductivity is the major contribution to the thermal conduction of these clathrate materials. For $Sr_8Zn_8Ge_{38}$, the comparable electronic and lattice components of the thermal conductivity show that both electrons and phonons play an important role in its thermal conductivity.

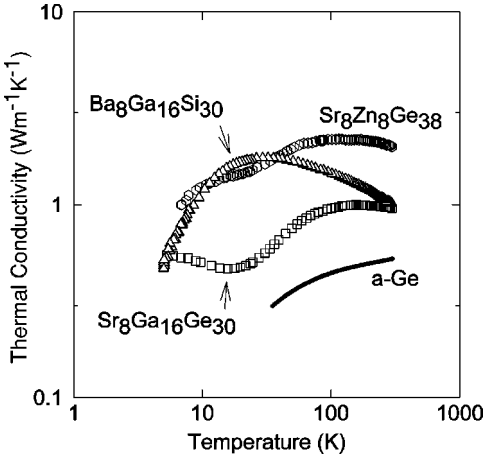

FIG. 9. Thermal conductivities of $Ba_8Ga_{16}Si_{30}$, $Sr_8Zn_8Ge_{38}$, $Sr_8Ga_{16}Ge_{30}$, and amorphous Ge.

IV. CONCLUSIONS

The structural parameters, thermal and transport properties of three clathrates, $Sr_8Zn_8Ge_{38}$, $Sr_8Ga_{16}Ge_{30}$ and $Ba_8Ga_{16}Si_{30}$, have been determined below room temperature. The emerging picture is that a looser fit of the guest in a more flexible cage is associated with low-frequency rattling of the guest atoms, and leads to higher volume thermal expansion coefficients, anomalously high low-temperature values of the Grüneisen parameter, and low glasslike thermal conductivity, dictated by short phonon mean free paths.

ACKNOWLEDGMENTS

The support to L.Q. from NSERC is gratefully acknowledged. G.S.N. gratefully acknowledges support from the University of South Florida and M.A.W. gratefully acknowledges financial support from NSERC and Killam Trusts.

[1] J. S. Kasper, P. Hagenumuller, M. Pouchard, and C. Cros, Science **150**, 1713 (1965).
[2] P. Mélinon, P. Keghélian, A. Perez, B. Chamoagnon, Y. Guyot, L. Saviot, E. Reny, C. Cros, M. Pouchard, and A. Dianoux, Phys. Rev. B **59**, 10 099 (1999).
[3] J. S. Tse, K. Uehara, R. Rousseau, A. Ker, C. I. Ratcliffe, M. A. White, and G. MacKay, Phys. Rev. Lett. **85**, 114 (2000); **86**, 4980 (2001).
[4] G. S. Nolas, J.-M. Ward, J. Gryko, L. Qiu, and M. A. White, Phys. Rev. B **64**, 153201 (2001).
[5] G. S. Nolas, T. J. R. Weakley, J. L. Cohn, and R. Sharma, Phys. Rev. B **61**, 3845 (2000).
[6] G. S. Nolas, B. C. Chakoumakos, B. Mahieu, G. L. Long, and T. J. R. Weakley, Chem. Mater. **12**, 1947 (2000).
[7] G. S. Nolas, J. L. Cohn, G. A. Slack, and S. B. Schujiman, Appl. Phys. Lett. **73**, 178 (1998).
[8] J. D. Bryan, V. I. Srdanov, G. D. Stucky, and D. Schmidt, Phys. Rev. B **60**, 3064 (1999).
[9] J. L. Cohn, G. S. Nolas, V. Fessatidis, T. H. Metcalf, and G. A. Slack, Phys. Rev. Lett. **82**, 779 (1999).
[10] G. S. Nolas, T. J. R. Weakley, and J. L. Cohn, Chem. Mater. **11**, 2470 (1999).
[11] B. C. Chakoumakos, B. C. Sales, D. G. Mandrus, and G. S. Nolas, J. Alloys Compd. **296**, 80 (2000).
[12] J. S. Tse and M. A. White, J. Phys. Chem. **92**, 5006 (1988).
[13] B. B. Iversen, A. E. C. Palmqvist, D. E. Cox, G. S. Nolas, G. D. Stucky, N. P. Blake, and H. Metiu, J. Solid State Chem. **149**, 455 (2000).
[14] G. S. Nolas, G. A. Slack, and S. B. Schujiman, *Semiconductor Clathrates: A Phonon-Glass Electron-Crystal Material with Potential for Thermoelectric Applications*, in *Semiconductors and Semimetals*, edited by T. M. Tritt (Academic, New York, 2001), Vol. 69, p. 255.
[15] L. Qiu, M. A. White, Z. Li, J. S. Tse, C. I. Ratcliffe, C. A. Tulk, J. Dong, and O. F. Sankey, Phys. Rev. B **64**, 024303 (2001).
[16] M. J. M. Van Oort and M. A. White, Rev. Sci. Instrum. **58**, 1241 (1987).
[17] N. P. Blake, D. Bryan, S. Latturner, L. Møllnitz, G. D. Stucky, and H. Metiu, J. Chem. Phys. **114**, 10063 (2001).
[18] Y. Zhang, P. L. Lee, G. S. Nolas, and A. P. Wilkinson, Appl. Phys. Lett. **80**, 2931 (2002).
[19] K. Moriguchi, S. Munetoh, A. Shintani, and T. Motooka, Phys. Rev. B **64**, 195409 (2001).
[20] L. W. Finger, VOLCAL (Code Modification 10/18/96), Carnegie Institute of Washington, Geophysical Laboratory, Washington, DC, 1971.
[21] T. B. Žunić and I. Vicković, J. Appl. Crystallogr. **29**, 305 (1996).
[22] B. C. Sales, D. G. Mandrus, and B. C. Chakoumakos, *Semiconductors and Semimetals* (Academic, New York, 2001), Vol. 70, p. 1.
[23] G. S. Nolas and C. A. Kendzioora, Phys. Rev. B **62**, 7157 (2000).
[24] D. F. Gibbons, Phys. Rev. **112**, 136 (1958).
[25] I. Ibach, Phys. Status Solidi **31**, 625 (1969).
[26] J. S. Tse, W. R. McKinnon, and M. Marchi, J. Phys. Chem. **91**, 4188 (1987).
[27] J. F. Meng, N. V. C. Shekar, J. V. Badding, and G. S. Nolas, J. Appl. Phys. **89**, 1730 (2001).
[28] A. San-Minguel, P. Kéghélian, X. Blasé, P. Mélinon, A. Perez, J. P. Itié, A. Polian, E. Reny, C. Cros, and M. Pouchard, Phys. Rev. Lett. **83**, 5290 (1999).
[29] J. S. Tse, J. Phys. (Paris), Colloq. **48**, Cl-543 (1987).
[30] D. G. Cahill, S. K. Watson, and R. O. Pohl, Phys. Rev. B **46**, 6131 (1992).
[31] G. A. Slack and S. Galginaitis, Phys. Rev. **133**, A253 (1964).